DOI: 10.1002/ejic.201000838

Iron(III)-Pivalate-Based Complexes with Tetranuclear $\{Fe_4(\mu_3\text{-}O)_2\}^{8+}$ Cores and *N*-Donor Ligands: Formation of Cluster and Polymeric Architectures

Svetlana G. Baca,*[a] Irina G. Filippova,[b] Tony D. Keene,[c] Olga Botezat,[a] Iurii L. Malaestean,[a] Helen Stoeckli-Evans,[d] Victor Ch. Kravtsov,[b] Iurii Chumacov,[b] Shi-Xia Liu,*[c] and Silvio Decurtins[c]

Keywords: Coordination polymers / Iron / Carboxylate ligands / N ligands / Magnetic properties

Different synthetic routes have been used for the preparation of a new tetranuclear $[Fe_4O_2(O_2CCMe_3)_8(bpm)]$ cluster (**1**) and a one-dimensional coordination polymer $[Fe_4O_2(O_2CCMe_3)_8(hmta)]_n$ (**2**) (bpm = 2,2′-bipyrimidine and hmta = hexamethylenetetramine). For cluster **1**, two structural isomers, **1a** and **1b**·3MeCN, have been found. X-ray crystallographic analysis showed that all complexes consist of a central $\{Fe_4(\mu_3\text{-}O)_2\}^{8+}$ core. In **1a**, metal ions in the core are additionally linked by six bridging pivalates as two other pivalates and a bpm ligand are chelated to Fe^{III} ions, whereas in cluster **1b**, metal ions in the $\{Fe_4(\mu_3\text{-}O)_2\}^{8+}$ core are linked by seven bridging pivalates and only one carboxylate as well as bpm are chelated to the iron centers. In coordination polymer **2**, $[Fe_4O_2(O_2CCMe_3)_8]$ clusters are bridged by hmta ligands to form zigzag chains. Magnetic measurements have been carried out to characterize these complexes and revealed antiferromagnetic interactions between Fe^{III} ions with best-fit parameters of J_{wb} = –72.2 (**1a**) and –88.7 cm^{-1} (**1b**) for wing···body interactions.

Introduction

During the last decade, there has been tremendous interest in the synthesis, investigation, and possible applications of coordination polymers or inorganic–organic hybrid materials.[1] As they possess unprecedented electrical, optical, magnetic, biological, and catalytic properties, the coordination polymers represent strategic and revolutionary materials that find extensive uses in science and nanotechnology. The fields of possible application include adsorption, storage, separation, catalysis, luminescence, magnetism, and conductivity. Moreover, with increasing demand for alternative sources of energy, the fabrication of new coordination polymers has been driven by the rapid growth of their practical use as materials for energy storage and the conversion, storage, and transport of hydrogen, methane, and oxygen.[2] Some new research fields have opened in which coordination polymers have been used; they include the development of new magnetic coordination polymers due to their great potential in the formation of "intelligent" multifunctional materials, magnetic sensors, and magnetic materials, in particular as future spintronic devices.[3]

The most promising approach to the construction of coordination polymers based on building blocks is the so-called bottom-up assembly.[4] Coordination polymers can be designed and synthesized by the choice of appropriate preorganized metal-ion-containing building blocks and bridging ligands that differ by size, shape, charge, and functionalities. Transition-metal clusters are versatile building blocks that can be used for the generation of numerous molecular magnetic frameworks. Moreover, some of them can behave as "single molecule magnets" (SMMs)[5] and exhibit slow thermal and quantum relaxation of magnetization below a so-called blocking temperature. However, despite the characterization of numerous polynuclear clusters, including those that exhibit SMM properties, surprisingly little analogous work has been done to build magnetic coordination polymers through the linking of high-nuclearity metal-ion clusters. Networks of metal-ion clusters bridged by appropriate ligands can result in stronger magnetic interactions than what is achievable without such bonding, thereby resulting in much more pronounced magnetic effects, and the construction of such materials is currently a challenging target.

Recently, we have reported the synthesis and characterization of one-dimensional manganese chain coordination polymers composed of cluster blocks such as $\{Mn_3\}$, $\{Mn_3O\}$, and $\{Mn_4O_2\}$ bridged by 2,2′-bipyrimidine (bpm) or hexamethylenetetramine (hmta) ligands to give

[a] Institute of Chemistry, ASM,
Academiei 3, 2028 Chisinau, R. Moldova
E-mail: sbaca_md@yahoo.com
[b] Institute of Applied Physics, ASM,
Academiei 5, 2028 Chisinau, R. Moldova
[c] Department of Chemistry and Biochemistry, University of Bern,
Freiestrasse 3, 3012 Bern, Switzerland
E-mail: liu@iac.unibe.ch
[d] Institut de Microtechnique, Université de Neuchâtel,
Rue Jaquet Droz 1, 2002 Neuchâtel, Switzerland
Supporting information for this article is available on the WWW under http://dx.doi.org/10.1002/ejic.201000838.

$\{[Mn_3(O_2CCHMe_2)_6(bpm)]\cdot 2EtOH\}_n$, $[Mn_4O_2(O_2CCHMe_2)_6(bpm)(EtOH)_4]_n$, and $\{[Mn_3O(O_2CCHMe_2)_6(hmta)_2]\cdot EtOH\}_n$.[6] Thereby, using a combination of vector coupling and full-matrix diagonalization techniques, a good estimation of the intercluster coupling strength in the manganese coordination polymers between both linear $\{Mn_3\}$ cores and μ-oxo trinuclear $\{Mn_3O\}$ cores, and for which no model was previously reported, has been given. In continuation of this work, we extended our study on iron polynuclear carboxylate systems and present here the synthetic routes to a new butterfly-like $[Fe_4O_2(O_2CCMe_3)_8(bpm)]$ cluster (**1**) that contains a chelating bpm molecule [this cluster shows two structural isomers (**1a** and **1b**)] and a one-dimensional coordination polymer composed of $[Fe_4O_2(O_2CCMe_3)_8]$ clusters bridged by hmta ligands, namely, $[Fe_4O_2(O_2CCMe_3)_8(hmta)]_n$ (**2**). X-ray crystallography and magnetic measurements have been carried out to characterize these complexes.

Only a few examples of iron coordination polymers built from polynuclear cluster blocks have been reported in the literature. This includes a zigzag chain coordination polymer $[Fe_3O(O_2CCMe_3)_6(H_2O)(dca)]_n$, in which $[Fe_3O(O_2CCMe_3)_6]$ units are linked by 1,5-dicyanamide (dca) ligands;[7] a helical polymer of Fe^{II} centers that are linked through 6-chloro-1-pyridinol (Hchp) and acetate ligands in $[Fe_9(chp)_{12.4}(O_2CMe)_{5.6}]_n$;[8] and a two-dimensional coordination polymer $[Fe_{10}O_4(OMe)_{14}Cl_4(mcce)]$ (mcce = 2-carbamoyl-2-cyanoethanimidate) composed of antiferromagnetically coupled $\{Fe_{10}\}$ clusters.[9]

Results and Discussion

Syntheses

Many synthetic routes to polynuclear carboxylate complexes rely on using predesigned clusters such as trinuclear μ3-oxo-bridged carboxylate complexes $[M_3O(O_2CR)_6L_3]^{+/0}$ with organic ligands. We explored this synthetic procedure for preparing a tetranuclear $[Fe_4O_2(O_2CCMe_3)_8(bpm)]$ cluster (**1a**) and a coordination polymer $[Fe_4O_2(O_2CCMe_3)_8(hmta)]_n$ (**2**). The reaction of the μ3-oxo trinuclear pivalate complex $[Fe_3O(O_2CCMe_3)_6(H_2O)_3]Me_3CCO_2\cdot 2Me_3CCO_2H$ with 2,2′-bipyrimidine in CH_2Cl_2/MeCN gave a deep red-brown solution from which complex **1a** was isolated in around 60% yield. Complex **1a** can also be made by microwave irradiation and crystalline material appears after five days in higher yields (ca. 80%). Treatment of trinuclear μ3-oxo iron pivalate with a MeCN solution of hexamethylenetetramine formed a precipitation of coordination polymer **2** (yield ca. 35%) in which butterfly tetranuclear clusters $[Fe_4O_2(O_2CCMe_3)_8]$ bridged by hmta ligands form zigzag chains. In contrast, using a hexanuclear $[Fe_6O_2(OH)_2(O_2CCMe_3)_{12}]$ cluster as a starting material and a similar preparative procedure (both in solution and under microwave heating) afforded solvated $[Fe_4O_2(O_2CCMe_3)_8(bpm)]$ (**1b**·3MeCN). Employment of the microwave-assisted reaction in the preparation of **1b** clearly improves its yield (56%) in comparison with the solution method (22%).

Spectroscopic Measurements

The infrared spectra of all complexes **1a**, **1b**, and **2** have strong and broad bands in the 1566–1548 and 1420–1407 cm^{-1} regions, which arise from asymmetric and symmetric vibrations of the coordinated carboxylate groups of the pivalate ligands, respectively.[10] The ν(C=N) stretching vibrations for bpm[11] are also observed in this region and these overlap with the asymmetric stretching bands of the carboxylates. The C–H asymmetric and symmetric stretching vibrations for the *tert*-butyl group of pivalates are observed in the range of 2961–2869 cm^{-1}, along with a strong single band at 1483–1481 cm^{-1} and a doublet at 1376–1360 cm^{-1}, which correspond to asymmetric and symmetric bending vibrations for methyl, respectively. In the case of complex **2**, several well-separated strong and sharp bands at 1251, 1056, 1024, and 987 cm^{-1} can be assigned to the C–N stretching modes of the coordinated hmta.[12]

Thermogravimetric Studies

Thermogravimetric analyses for all complexes were performed under a nitrogen atmosphere in the temperature range of 25–600 °C. The TGA data show that for compound **1a**, a first weight loss is observed from 220 to 300 °C that corresponds to the removal of a bpm molecule (found 12.4%, calcd. 12.9%). Complex **1b** loses three solvate acetonitrile molecules and a bpm ligand in two steps from 100 to 300 °C (the total weight loss is 20.2%, calcd. 20.95%). On further heating, in the temperature range of 300–600 °C the decomposition of eight pivalic molecules takes place in three steps with a total weight loss of 64.8% for **1a** (calcd. 66.2%) and 56.8% for **1b** (calcd. 60.1%) to the final product (found: 22.7% for **1a** and 22.9% for **1b**; calcd. 26.1% for **1a** and 23.7% for **1b**). The coordination polymer **2** is stable up to 200 °C and then it loses weight (32.8%), which corresponds to the release of three carboxylate ligands (calcd. 33.6%). The decomposition of a hmta ligand and five remaining pivalic ligands occurs above 300 °C in two steps with the total weight loss of 52.7% (calcd. 53.6%) and is completed below 600 °C to give the expected oxide (found 14.6%, calcd. 13.3%).

Structural Characterization

The Cambridge Structural Database (version 5.29)[13] includes 27 tetranuclear Fe^{III} oxo-bridged carboxylate complexes with the $\{Fe_4(\mu_3\text{-}O)_2\}^{8+}$ core.[14–36] This well-known tetranuclear core comprises an innermost planar or almost planar entity of two (so-called "body") Fe atoms doubly bridged by two μ3-oxo atoms, connected outwards to the remaining ("wings") Fe atoms. The iron butterfly complexes can be also considered to consist of two edge-sharing $\{Fe_3(\mu_3\text{-}O)\}$ triangular subunits. Tetranuclear complexes with $\{Fe_4(\mu_3\text{-}O)_2\}^{8+}$ cores show different configurations depending on the arrangement of the four Fe atoms and the displacement of the $(\mu_3\text{-}O)_2$ ions relative to their respective

Fe_3 planes. Three types of Fe^{III} atom dispositions in the $\{Fe_4(\mu_3\text{-}O)_2\}^{8+}$ core have been most often discussed.[14–16] There are "bent," "planar," and "chairlike" types (Scheme 1). The latter is a hybrid of the first two forms and has been rarely observed. The pyramidal μ_3-O ions lie on the same sides of Fe_3 planes in bent cores and on the opposite sides in planar and chairlike variants. Sometimes it is difficult to distinguish the planar and chairlike forms from each other by the values of deviation from ideal Fe_4 planes or the degree of pyramidality of μ_3-O ions. For example, complexes $[Fe_4O_2Cl_2(O_2CMe)_2\{(py)_2CNO\}_4]$ and $[Fe_4O_2(N_3)_2(O_2CMe)_2\{(py)_2CNO\}_4]$ in the literature[16] were described as chairlike, but their four Fe atoms have an almost planar arrangement [their average displacements from the ideal plane are ca. 0.02 and 0.01 Å, respectively]. There is an alternative way for the description of the conformations.[17] The iron butterfly complexes are subdivided into two distinct forms [type **I** and type **II**]. These types are distinguished by the position of the two external atoms relative to the central Fe_2O_2 plane. For type **I** complexes, the two wing Fe atoms lie on the same side (*cis*) of the Fe_2O_2 plane, and for type **II**, the wings of Fe atoms are *trans* relative to the Fe_2O_2 plane. Accordingly, the μ_3-O atoms sit on the same side (**I**) or on opposite sides (**II**) of the mean plane that passes through all four iron atoms.

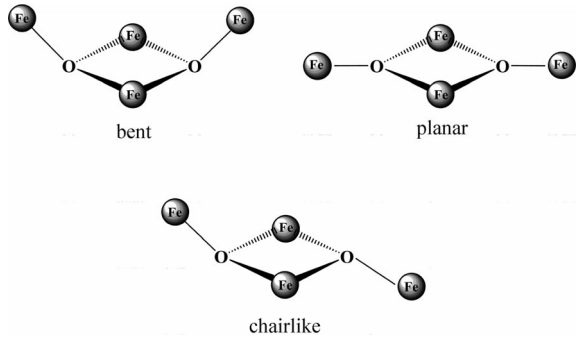

Scheme 1. Three types of butterfly configurations.

A detailed analysis of the geometries of the $\{Fe_4(\mu_3\text{-}O)_2\}^{8+}$ core is presented in the literature, especially in ref.[18] but also in ref.[16,19–23]. We have summarized several characteristic data of these compounds in Table 1. The comparison of Fe···Fe contacts, and Fe–O distances and angles of the Fe^{III} entity reveals a remarkable structural similarity. Two compounds, $[\mathbf{L}_2Fe_4(\mu_3\text{-}O)_2(\mu_2\text{-}MeCO_2)_3(sao)_2]PF_6$[22] and $[\mathbf{L}_2Fe_4(\mu_3\text{-}O)_2(Ph_2C(OH)CO_2)_3(sao)_2]$ (ClO_4),[25] in which **L** = 1,4,7-trimethyl-1,4,7-triazacyclononane and H_2sao = salicylaldoxime, are the exceptions from this family. They have atypical values of both bond lengths and angles as well as unusual conformations of their basic cores. The bridging oxo atoms sit almost in the Fe_3 planes. These distortions may be due to the existence of an asymmetric N,O bridge in the H_2sao ligand.

$[Fe_4O_2(O_2CCMe_3)_8(bpm)]$ (1a and 1b)

Compounds **1a** and **1b** have the same composition of the $[Fe_4O_2(O_2CCMe_3)_8(bpm)]$ cluster moiety but differ by the function of one pivalate carboxylate group, the connectivity of the ligands, and the solvent molecules. The molecular structure of **1a** is presented in Figure 1 (a), selected interatomic distances and angles are given in Table 2, and a packing diagram is shown in the Supporting Information (Figure S1). As seen in Figure 1 (a), the Fe1 and Fe3 atoms occupy the body sites and Fe2 and Fe4 atoms reside in the wingtip sites. The two body ions bridged by two μ_3-oxides have an Fe1···Fe3 separation of 2.909(1) Å. Similar distances may be found in $\{Fe_4O_2\}$-core-based complexes even if they do not have an additional bridge between the body atoms; see, for example, in other reported works[18,26–27] (Table 1). The four Fe atoms in **1a** (Figure 2) are coplanar within 0.099 Å and the μ_3-oxygen atoms O1 and O2 occupy opposite positions from this plane. The dihedral angle between the planes Fe1/Fe3/Fe2 and Fe1/Fe3/Fe4 is 172.9°. The O1 and O2 atoms deviate from these planes by 0.454 and 0.460 Å, respectively, thus having a flattened pyramidal arrangement of bonds.

Each iron atom is six-coordinate and has a distorted octahedral coordination sphere. The Fe1, Fe3, and Fe4 ions are all O_6-coordinated: the Fe1 atom is coordinated by two μ_3-oxo atoms and four oxygen atoms from pivalate ligands (two bridging and one chelating); the Fe3 atom is bonded to two μ_3-oxo atoms and four oxygen atoms from bridging pivalates; the Fe4 atom is ligated by a μ_3-oxygen atom, three oxygen atoms from bridging pivalates, and two oxygen atoms from a chelating carboxylate. The Fe2 atom has an N_2O_4 coordination environment that arises from a μ_3-oxygen atom, a chelating bpm molecule, and three bridging pivalate ligands. The Fe–O distances fall in the range of 1.829(1)–2.081(2) Å, and the Fe–N bonds are 2.184(2) and 2.213(2) Å. The wingtip iron atoms form two short bonds [Fe2–O1 1.829(1) and Fe4–O2 1.834(1) Å] with μ_3-O^{2-} ions. The innermost Fe_2O_2 entity reveals two short [1.931(1) and 1.932(2) Å] and two long [1.962(2) and 1.963(1) Å] bond lengths. Six pivalate ligands exhibit an identical bidentate μ_2-bridging function, whereas two other carboxylate groups are chelating and bind to the Fe1 and Fe4 atoms (Figure 2). These four-membered chelate cycles as well as the bpm ligand provoke significant deviations from an octahedral geometry in the body Fe1 atom and both wingtip Fe2 and Fe4 atoms. The angles O17–Fe4–O18, O16–Fe1–O15, and N4–Fe2–N1 being 61.57(6), 62.99(6), and 74.21(6)°, respectively, are far from the ideal octahedral angle. The longest Fe–O distances [2.174(2) and 2.101(2) Å] belong to chelating carboxylate groups. The body/wingtip Fe···Fe distances are of two kinds, those bridged by one pivalate group [Fe1···Fe2 3.360(1) Å, Fe1···Fe4 3.376(1) Å] and those bridged by two pivalate ligands [Fe3···Fe2 3.273(1) Å, Fe3···Fe4 3.264(1) Å].

The asymmetric unit of **1b** contains two similar complexes. The molecular structure of one of them (complex A) is shown in Figure 1 (b), selected interatomic distances and angles are given in Table 3, and a packing diagram of **1b** is shown in the Supporting Information (Figure S2). Unlike **1a**, only one pivalate molecule acts as a chelate ligand and the other seven have bidentate bridging functions. More-

Table 1. Comparison of selected structural parameters of $[Fe_4O_2]^{8+}$ core and magnetic interactions.

	Complex and CCDC refcode	Type of butterfly configuration	Fe_b–Fe_b [Å]	Fe_b–Fe_w [Å]	Fe_w–Fe_w [Å]	Fe_b–μ_3–O [Å]	Fe_w–μ_3–O [Å]	Fe_b–μ_3–O–Fe_b [°]	Fe_w–μ_3–O–Fe_b [°]	O–Fe_b–O [°]	Dihedral angle between Fe_3 planes [°]	Deviations of μ_3-O atoms from Fe_3 planes (absolute value) [Å]	Sum of angles around μ_3-O [°]	J [cm^{-1}]	Ref.
Benzoates															
1.	$(Et_4N)[Fe_4O_2(O_2CPh)_7(H_2B(pz)_2)_2]\cdot 2CH_2Cl_2$ (FORYIU)	bent	2.829	3.326 3.330 3.488 3.500	5.920	1.895 1.917 1.955 1.967	1.822 1.854	93.5 94.5	125.1 125.9 133.6 134.1	85.4 85.6	144.8	0.27 0.28	353.2 353.5	no	[19]
2.	$[Fe_4O_2(bicoH)_2(bico)_2(O_2CPh)_4]Cl_2\cdot 5H_2O\cdot 2MeCN$ (FURPOX)	planar	2.90	3.29 3.59	6.25	1.94 1.97	1.884	95.7	119.0 136.8	84.3	180	0.31 0.31	351.5	no	[18]
3.	$[Fe_4O_2(O_2CPh)_7(phen)_2](ClO_4)\cdot 2MeCN$ (VAFLAQ)	bent	2.879	3.296 3.472 3.458 3.302	5.880	1.925 1.934 1.959 1.916	1.819 1.807	96.5 96.0	134.2 123.7 124.5 134.3	82.9 83.8	147.6	0.24 0.25	354.8 354.4	$J_{wb} = -77.6$ $J_{bb} = -2.4$	[26]
4.	$[Fe_4O_2(O_2CPh)_7(phen)_2]\cdot 2H_2O$ (VAFLEU)	bent	2.913	3.456 3.275	5.780	1.931 1.961	1.821	96.9	121.6 132.1	83.0	144.3	0.33	350.6	$J_{wb} = -65.7$ $J_{bb} = -15.6$	[26]
Pivalates															
5.	$[Fe_4O_2(O_2CCMe_3)_8(2\text{-Me-5-Etpy})_2]\cdot 2MeCN$ (QILKIF)	planar	2.942	3.314 3.317	5.943	1.931 1.936	1.836	99.1	123.1 123.2	80.9	180	0.42 0.42	345.3		[27]
			2.952	3.320 3.314	5.941	1.936 1.929	1.841	99.6	123.04 123.07	80.37	180	0.41 0.41	345.7	no	
6.	$[Fe_4O_2(O_2CCMe_3)_8(2\text{-Me-py})_2]\cdot 2MeCN$ (OMAJUH)	planar	2.951	3.333 3.346	5.992	1.940 1.942	1.853	98.96	122.85 123.79	81.04	180	0.42 0.42	345.6	$J_{wb} = -37.2$	[17]
Trifluoroacetates															
7.	$[Fe_4O_2(O_2CCF_3)_8(H_2O)_6]\cdot 2H_2O$ (CINRIA)	planar	2.915	3.436 3.476	6.276	1.961 1.936	1.842	96.5	133.9 129.5	82.9	180	0.04 0.04	359.9	no	[28]
8.	$[Fe_4O_2(O_2CCF_3)_8(bpy)_2]\cdot CF_3CO_2H$ (EMIGAI)	bent	2.893	3.306 3.474 3.313 3.450	5.933	1.916 1.953 1.922 1.960	1.840 1.837	96.8 96.4	123.75 130.90 132.34 123.16	83.39 83.44	151.3	0.31 0.31	351.5 351.9	no	[29]
9.	$[Fe_4O_2(O_2CCF_3)_8(dmf)_4]$ (CIDLUX)	bent	2.900	3.394 3.435	5.968	1.940 1.936	1.862	96.9	126.64 129.24	83.06	149.7	0.29 0.29	352.8	no	[30]
Acetates															
10.	$[Fe_4O_2(O_2CMe)_7(bpy)_2]\cdot ClO_4\cdot 1/4CH_2Cl_2\cdot H_2O$ (VIVDAF)	bent	2.855	3.306 3.439	5.738	1.926 1.947	1.819	95.0	131.99 123.9	84.5	139.6	0.32 0.32	350.8	$J_{wb} = -45.5$ $J_{bb} = -8.9$	[20]
11.	$[Fe_4O_2(O_2CMe)_7(bpy)_2]\cdot Cl$ (LAWFOE)	bent	2.855	3.301 3.442	5.750	1.922 1.941	1.821	95.3	123.73 132.36	84.14	140.4	0.31 0.31	351.4	no	[31]
12.	$[Fe_4O_2Cl_2(O_2CMe)_6(bpy)_2]$ (PUDCEW)	chair	2.895	3.234 3.421 3.486 3.393	5.805	1.993 1.937 1.932 1.994	1.810 1.823	94.9 95.0	119.33 128.19 129.28 131.94	84.02 81.02	143.6	0.46 0.21	356.2 342.4	$J_{wb} = -4.1$ $J_{bb} = -10.9$	[14]
13.	$[n\text{Bu}_4\text{N}][Fe_4O_2(O_2CMe)_7(pic)_2]$ (PUDCIA)	bent	2.842	3.315 3.477 3.332 3.463	5.784	1.912 1.941 1.914 1.954	1.844	95.0 94.6	133.40 123.78 125.03 131.52	84.64 84.23	139.1	0.32 0.30	352.2 351.2	no	[14]
14.	$[Fe_4O_2(O_2CMe)_6Cl_2(3\text{-Mepy})_4]\cdot MeCN$ (LALGOU)	bent	2.898	3.340 3.446 3.456 3.322	6.016	1.924 1.951 1.950 1.924	1.854 1.856	96.8 96.8	124.3 129.8 130.5 123.0	83.0 83.0	157.6	0.33 0.34	350.3 350.9	no	[32]

Table 1. *(Continued)*

15.	$[Fe_4O_2(O_2CMe)_6(py)_4Cl_2]$ (POYMUL)	bent	2.878	3.316 3.462	6.033	1.907 1.945	1.861	96.7	123.2 130.9	83.1	158.6	0.33 0.33	350.8	no	[23]
16.	$[Fe_4O_2(O_2CMe)_7(C_{10}H_9N_3)_2(H_2O)]Cl\cdot1.25EtOH\cdot H_2O$ (CELFOP)	bent	2.924	3.299 3.420 3.413 3.334	5.884	1.915 1.956 1.933 1.986	1.828 1.820	98.2 96.6	128.82 123.64 125.24 127.83	82.77 82.47	151.9	0.33 0.35	350.6 349.6	no	[33]
17.	$[Fe_4O_2(O_2CMe)_6(N_3)(phen)_2]\cdot3MeCN$ (IVUXOM)	chair	2.884	3.426 3.272 3.446 3.416	6.001	1.963 1.940 1.983 1.931	1.810 1.844	95.3 94.9	121.4 130.4 128.5 129.6	84.4 82.5	156.2	0.39 0.29	353.0 347.1	$J_{wb} = -70$ $J_{bb} = -11$	[15]
18.	$[Fe_4O_2Cl_2(O_2CMe)_2\{(py)_2CNO\}_4]2CH_2Cl_2\cdot2.5H_2O$ (DEQKAM)	chair	2.887	3.377 3.264 3.366 3.259	5.967	1.897 1.991 1.895 1.986	1.882 1.882	95.9 96.1	114.8 126.7 114.9 126.0	81.5 86.4	178.4	0.53 0.53	337.4 336.9	$J_{wb} = -40.2$ $J_{bb} = -59.4$	[16]
19.	$[Fe_4O_2(N_3)_2(O_2CMe)_2\{(py)_2CNO\}_4]\cdot2CH_2Cl_2\cdot H_2O$ (DEQJOZ)	chair	2.916	3.362 3.269 3.385 3.255	5.956	1.904 1.974 1.912 1.980	1.895 1.877	97.5 97.0	115.3 124.5 115.1 126.6	81.0 84.5	179.5	0.53 0.51	337.3 338.5	no	[16]
20.	$[Fe_4O_2Cl_2(O_2CMe)_2\{(py)_2CNO\}_4]\ 4.5MeNO_2$ (DEQJUF)	chair	2.890	3.254 3.398 3.260 3.371	5.968	1.918 1.978 1.906 1.993	1.855 1.875	95.8 95.7	114.8 126.7 114.9 126.2	86.1 82.2	177.5	0.53 0.64	337.3 336.7	no	[16]
21.	$[Fe_4O_2(mcpa)_6Cl_2(py)_4]\cdot2MeCN$ (DEWQOM)	bent	2.902	3.473 3.345 3.341 3.478	6.116	1.950 1.918 1.914 1.950	1.863 1.869	97.2 97.4	124.4 131.2 124.1 131.3	82.2 82.3	164.5	0.29 0.29	352.7 352.9	no	[34]
Propionates															
22.	$[Fe_4O_2(O_2CC_2H_5)_7(bpy)_2]\ ClO_4$ (PIZKAK)	bent	2.865	3.295 3.434 3.431 3.293	5.695	1.919 1.938 1.913 1.936	1.820 1.848	96.0 96.2	123.6 132.1 122.2 130.1	83.5 83.4	138.6	0.37 0.31	342.5 351.6	no	[35]
23.	$[Fe_4O_2(O_2CC_2H_5)_7(bpy)_2]\ ClO_4$ (PIZKAK01)	bent	2.865	3.294 3.432	5.695	1.918 1.938	1.817	95.9	123.7 132.0	83.3	138.6	0.31 0.31	351.7	no	[36]
24.	$Fe_4O_2(O_2CC_2H_5)_7(bpy)_2]PF_6\cdot2H_2O$ (QISDOL)	bent	2.874	3.444 3.306	5.714	1.953 1.924	1.824	95.7	123.8 131.5	83.6	138.5	0.32 0.32	351.0	$J_{wb} = -41.6$ $J_{bb} = -7.3$	[21]
Others															
25.	$\{[Fe_4O_2(2,4,5\text{-}T)_8(dmso)_4]\cdot2MeOH\cdot H_2O\cdot0.8dmso\}$ (NIBSIB)	bent	2.893	3.431 3.363	6.038	1.918 1.919	1.874	97.85	129.5 124.9	82.0	158.3	0.30 0.30	352.3	$J_{wb} = -69.7$ $J_{bb} = -5.6$	[24]
26.	$[L_2Fe_4O_2(MeCO_2)_3(sao)_2]PF_6$ (YAYPOD)	bent	2.839	3.625 3.241 3.709 3.214	6.100	1.910 2.019 2.068 1.888	1.827 1.891	92.54 91.62	112.0 154.9 111.0 154.7	87.3 85.3	150.8	0.15 0.07	357.3 359.4	$J_{wb} = -46$	[22]
27.	$[L_2Fe_4O_2(Ph_2C(OH)CO_2)_3(sao)_2](ClO_4)$ (WUTFIA)	bent	2.841	3.734 3.192 3.197 3.738	6.077	1.989 1.950 1.980 1.949	1.873 1.872	92.3 92.6	155.5 111.9 155.9 111.7	83.2 83.0	145.8	0.029 0.004	359.9 360.0	$J_{wb} = -41.4$	[25]
28.	$[Fe_4O_2(O_2CCMe_3)_8(bpm)]$ (**1a**)	chair	2.909	3.360 3.273 3.376 3.264	5.950	1.963 1.931 1.962 1.932	1.829 1.834	96.70 96.67	119.97 126.64 120.14 125.50	83.14 83.13	172.9	0.45 0.46	342.7 342.3	$J_{wb} = -72.2$	this work
29.	$[Fe_4O_2(O_2CCMe_3)_8(bpm)]$ (**1b**)	bent	2.867	3.408 3.279 3.292 3.443	5.588	1.956 1.905 1.950 1.944	1.803 1.833	96.2 94.4	122.6 128.9 122.6 132.7	84.4 83.5	134.0	0.38 0.34	349.7 347.7	$J_{wb} = -88.7$	this work
			2.866	3.408 3.289 3.400 3.274	5.471	1.937 1.949 1.913 1.945	1.850 1.800	96.2 94.8	122.6 130.4 121.0 128.3	83.9 83.2	129.8	0.37 0.41	347.8 345.4		
30.	$[Fe_4O_2(O_2CCMe_3)_8(hmta)]_n$ (**2**)	chair	2.855	3.311 3.323 3.402 3.440	6.015	1.897 1.906 1.968 1.970	1.803 1.821	97.3 92.9	127.2 127.0 127.6 130.4	83.3 83.6	160.5	0.31 0.32	351.5 350.9	no	this work

Subscripts: b = body, w = wingtip; phen = 1,10-phenanthroline; py = pyridine; bpy = 2,2'-bipyridine; pic = picoline; bicoh = bis(*N*-methylimidazol-2-yl)methanol]; $H_2B(pz)_2$ = dihydrobis(1-pyrazolyl)borate; 2-Me-5-Etpy = 5-ethyl-2-methylpyridine; 2-Mepy = 2-methylpyridine; 3-Mepy = 3-methylpyridine; $(py)_2CNO$ = di(2-pyridyl) ketone oxime; mcpa = 4-chloro-2-methylphenoxyacetate; 2,4,5-T = 2,4,5-trichlorophenoxyacetate; L = 1,4,7-trimethyl-1,4,7-triazacyclononane; H_2sao = salicylaldoxime.

over, **1a** and **1b** differ in their connectivity. The additional carboxylate bridge between the two body atoms Fe1 and Fe3 leads to shortening (in comparison with **1a**) of the Fe1···Fe3 distance up to 2.866(2) Å. In **1a**, two pairs of pivalate carboxylate groups bridge only one body iron atom (Fe3) with two iron atoms (Fe2 and Fe4) in the wing position, whereas in **1b** the double carboxylate bridges link each body iron atom with only one iron atom in the wing position. The Fe^{III} atoms in **1b** have a disordered octahedral coordination. In both complexes A and B, the Fe2 atom has a N_2O_4 coordination environment that arises from a chelating bpm ligand, three bridging pivalate ligands, and a μ_3-oxygen atom. The Fe1, Fe3, and Fe4 atoms are all O_6-coordinated: Fe1 and Fe3 are coordinated by two μ_3-oxygen atoms and four oxygen atoms from bridging pivalate ligands [three bridging and one chelating pivalates for Fe1 in **1a**], whereas Fe4 is coordinated by a μ_3-oxo atom, three oxygen atoms from bridging pivalate groups, and one oxygen from a chelating pivalate. The most significant deviations from octahedra are observed for the wingtip Fe2 and Fe4 atoms, which are coordinated by chelating bmp and pivalate ligands, respectively.

Table 2. Selected bond lengths [Å] and angles [°] in **1a**.

Fe1–O1	1.931(1)	Fe3–O1	1.962(2)	Fe1···Fe2	3.360(1)
Fe1–O2	1.963(1)	Fe3–O7	2.021(2)	Fe1···Fe4	3.376(1)
Fe1–O12	1.990(2)	Fe3–O4	2.018(2)	Fe2···Fe3	3.273(1)
Fe1–O13	2.017(2)	Fe3–O9	2.030(2)	Fe3···Fe4	3.264(1)
Fe1–O16	2.081(2)	Fe3–O6	2.036(2)	Fe2···Fe4	5.950(1)
Fe1–O15	2.101(2)	Fe4–O2	1.834(1)	O1–Fe1–O2	83.14(6)
Fe2–O1	1.829(1)	Fe4–O8	2.031(2)	O2–Fe3–O1	83.13(6)
Fe2–O5	1.976(2)	Fe4–O11	2.034(2)	Fe2–O1–Fe1	126.64(8)
Fe2–O3	2.031(2)	Fe4–O10	2.038(2)	Fe2–O1–Fe3	119.33(7)
Fe2–O14	2.052(1)	Fe4–O17	2.077(2)	Fe1–O1–Fe3	96.70(7)
Fe2–N4	2.184(2)	Fe4–O18	2.174(2)	Fe4–O2–Fe3	120.14(7)
Fe2–N1	2.213(2)			Fe4–O2–Fe1	125.50(7)
Fe3–O2	1.932(2)	Fe1···Fe3	2.909(1)	Fe3–O2–Fe1	96.67(7)

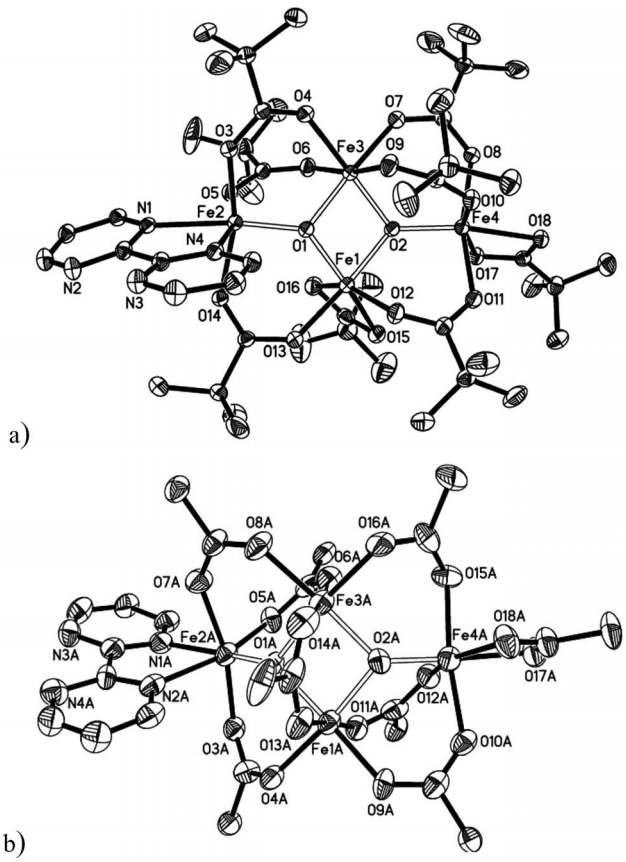

Figure 1. ORTEP representation of (a) complex **1a** and (b) one of the crystallographically independent complexes in **1b** at the 30% probability level. Hydrogen atoms, methyl groups, and solvent molecules in **1b** are omitted for clarity.

The difference in the coordination mode of the carboxylate ligand results in differences in the conformation of the $\{Fe_4O_2\}$ cores (Figure 2). The $\{Fe_4(\mu_3\text{-}O)_2\}^{8+}$ cores in **1b** have no crystallographically imposed symmetry, and this is also the case for **1a**. The wingtip Fe2 and Fe4 atoms deviate

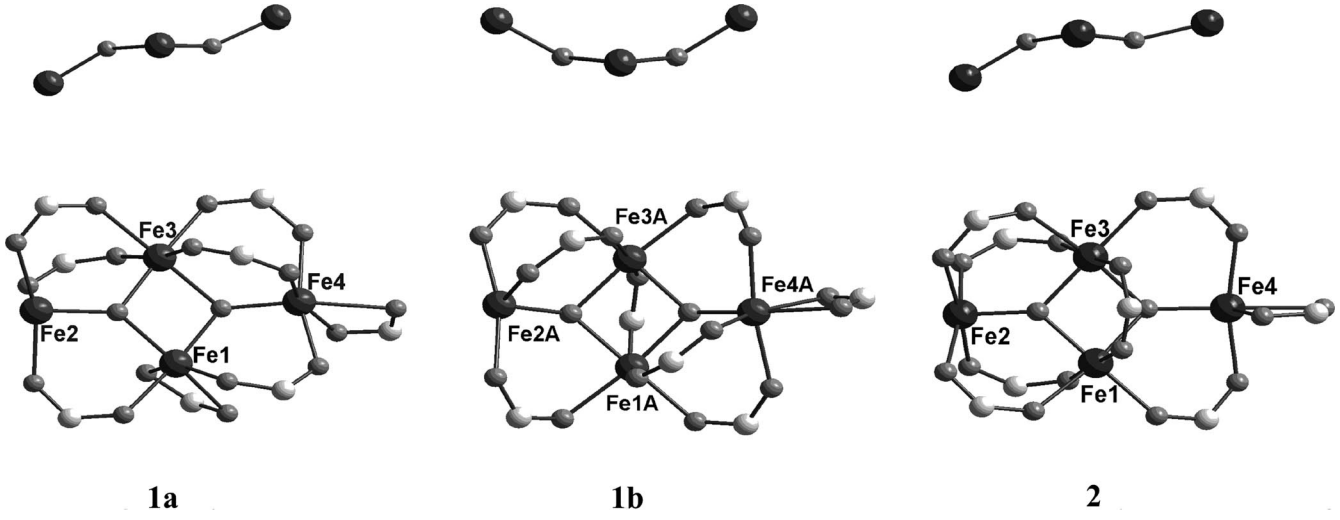

Figure 2. A back view of the Fe_4O_2 core (top) and tetranuclear metal core with coordinated carboxylate groups (bottom) in complexes **1a**, **1b**, and **2**. Hydrogen atoms, a bpm ligand, and Me_3C groups are omitted for clarity.

Table 3. Selected bond lengths [Å] and angles [°] in **1b**.

Fe1A–O1A	1.956(6)	Fe2B–O3B	1.980(7)
Fe1A–O2A	1.905(7)	Fe2B–O5B	1.983(8)
Fe1A–O9A	2.001(8)	Fe2B–O7B	2.023(7)
Fe1A–O4A	2.036(8)	Fe2B–O11B	2.054(8)
Fe1A–O13A	2.047(8)	Fe2B–N1B	2.162(1)
Fe1A–O11A	2.052(8)	Fe2B–N2B	2.179(1)
Fe2A–O1A	1.803(6)	Fe3B–O2B	1.937(7)
Fe2A–O5A	1.966(8)	Fe3B–O1B	1.949(8)
Fe2A–O7A	2.008(7)	Fe3B–O16B	1.985(9)
Fe2A–O3A	2.016(8)	Fe3B–O8B	2.015(7)
Fe2A–N2A	2.155(1)	Fe3B–O14B	2.046(7)
Fe2A–N1A	2.233(1)	Fe3B–O6B	2.064(7)
Fe3A–O2A	1.944(7)	Fe4B–O2B	1.850(7)
Fe3A–O1A	1.950(7)	Fe4B–O12B	1.956(8)
Fe3A–O16A	1.975(9)	Fe4B–O15B	2.004(8)
Fe3A–O14A	1.996(1)	Fe4B–O10B	2.029(8)
Fe3A–O8A	1.997(7)	Fe4B–O18B	2.057(8)
Fe3A–O6A	2.069(8)	Fe4B–O17B	2.148(9)
Fe4A–O2A	1.833(7)	Fe2B···Fe4B	5.471(2)
Fe4A–O12A	1.973(7)	Fe1A···Fe3A	2.867(2)
Fe4A–O15A	2.019(9)	Fe1A···Fe2A	3.443(2)
Fe4A–O10A	2.049(9)	Fe1A···Fe4A	3.279(2)
Fe4A–O18A	2.055(8)	Fe3A···Fe2A	3.292(2)
Fe4A–O17A	2.136(8)	Fe3A···Fe4A	3.408(2)
Fe1B–O1B	1.945(7)	Fe2A···Fe4A	5.588(2)
Fe1B–O2B	1.913(7)	Fe1B···Fe3B	2.866(2)
Fe1B–O9B	1.975(8)	Fe1B···Fe2B	3.400(2)
Fe1B–O4B	1.996(8)	Fe1B···Fe4B	3.274(2)
Fe1B–O13B	2.042(7)	Fe3B···Fe2B	3.289(2)
Fe2B–O1B	1.800(7)	Fe3B···Fe4B	3.406(2)
O2A–Fe1A–O1A	84.3(3)	Fe1A–O2A–Fe3A	96.2(3)
O2A–Fe3A–O1A	83.5(3)	Fe2A–O1A–Fe3A	122.6(4)
O2B–Fe1B–O1B	83.9(3)	Fe1B–O1B–Fe2B	130.4(3)
O2B–Fe3B–O1B	83.2(3)	Fe2B–O1B–Fe3B	122.6(3)
Fe1A–O1A–Fe2A	132.7(3)	Fe1B–O1B–Fe3B	94.8(3)
Fe3A–O1A–Fe1A	94.4(3)	Fe4B–O2B–Fe1B	121.0(3)
Fe4A–O2A–Fe1A	122.6(3)	Fe4B–O2B–Fe3B	128.2(4)
Fe3A–O2A–Fe4A	128.9(4)	Fe1B–O2B–Fe3B	96.2(3)

from the mean plane of the Fe_2O_2 core in the same direction at 1.047 and 1.161 Å for complex A, and 1.134 and 1.257 Å for complex B. The dihedral angles between planes through three iron atoms, each sharing the common μ_3-oxygen atoms, are 134.0 and 129.8° for complex A and B, respectively. The displacements of μ_3-oxygen atoms O1 and O2 from the corresponding planes of three Fe atoms equal 0.38 and 0.34 Å for complex A and 0.37 and 0.41 Å for complex B, respectively. The bent butterfly conformation leads to shorter Fe2···Fe4 contacts [5.471(2) and 5.588(2) Å] in **1b** compared with the same contact in **1a** [5.950(1) Å]. The Fe2–O1 and Fe4–O2 distances in **1b** are considerably unequal [1.803(6), 1.833(7) Å and 1.800(7), 1.850(7) Å for complexes A and B, respectively]. The Fe–ligand distances are quite similar to those in **1a** (see Tables 2 and 3).

$[Fe_4O_2(O_2CCMe_3)_8(hmta)]_n$ (2)

In the crystal structure of **2**, $[Fe_4O_2(O_2CCMe_3)_8]$ cluster moieties are linked into infinite zigzag chains by the bridging hmta ligand. Figure 3 shows a crystallographically independent repeating unit and a zigzag chain in **2**. The packing diagram of **2** is given in the Supporting Information (Figure S3). Four iron atoms are joined into a butterfly $\{Fe_4(\mu_3\text{-}O)_2\}^{8+}$ core by two μ_3-oxygen atoms and seven bidentate bridging pivalate ligands as in **1b**.

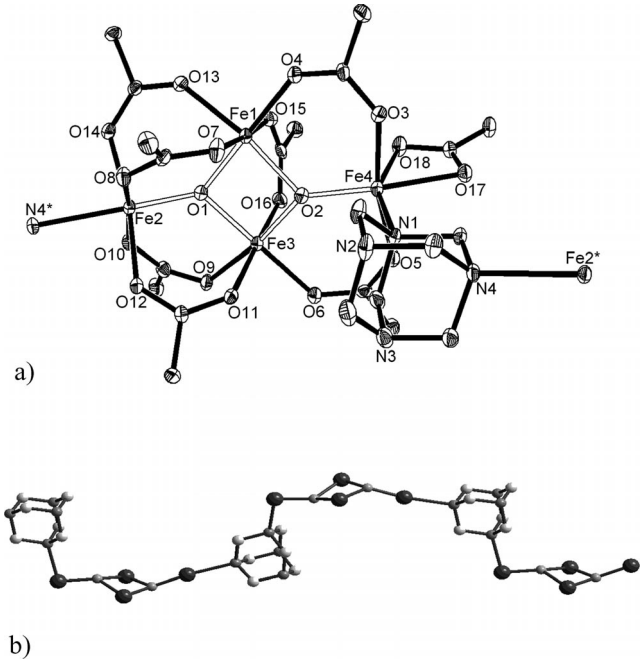

Figure 3. (a) ORTEP representation of complex **2** at the 50% probability level. Methyl groups and hydrogen atoms are omitted for clarity. (b) View of the chain along the *a* axis in **2**. Me_3CCO_2 groups and hydrogen atoms are omitted for clarity.

The coordination spheres of Fe1 and Fe3 are made of six oxygen atoms that come from four carboxylate groups and two μ_3-O atoms, whereas the wingtip Fe2 and Fe4 present a NO_5 distorted octahedral coordination that arises from one μ_3-O atom, one nitrogen atom of hmta, and four oxygen atoms of four bridging pivalate ligands (Fe2) or two bridging and one chelating pivalate ligand (Fe4). The bond lengths and angles in the coordination polyhedrons of iron atoms are listed in Table 4. The most significant distortions in the Fe octahedra are observed for wingtip iron atoms. The Fe2–O distances fall in the range of 1.803(4)–2.058(4) Å, whereas Fe2–N4 is distinctly longer and equals 2.350(5) Å. The small bite angle [62.1(2)°] of the chelate pivalate ligand distorts the coordination sphere of Fe4. The $\{Fe_4(\mu_3\text{-}O)_2\}^{8+}$ core is nonplanar and the Fe1/Fe2/Fe3 and Fe1/Fe3/Fe4 planes form a dihedral angle of 160.5°. Atoms O1 and O2 are displaced from these planes by 0.308 and 0.323 Å, respectively. The wingtip Fe2 atom is bridged by two pairs of carboxylate groups with the body atoms Fe1 and Fe3, whereas wingtip Fe4 is bridged to the body atoms Fe1 and Fe3 only by two single carboxylate groups (Figure 3). Therefore, the distances Fe2···Fe3 [3.311(1) Å] and Fe2···Fe1 [3.323(1) Å] are shorter than Fe4···Fe1 [3.402(2) Å] and Fe4···Fe3 [3.440(1) Å]. The inner Fe1 and Fe3 atoms have two oxo bridges and one carboxylate bridge. The distance between the iron atoms in the body positions is 2.855(2) Å and close to the lower edge of the range reported for $\{Fe_4O_2\}$ butterfly cores (Table 1).

Table 4. Selected bond lengths [Å] and angles [°] in **2**.

Fe1–O1	1.906(4)	Fe3–O2	1.968(4)	Fe1···Fe3	2.855(2)
Fe1–O2	1.970(4)	Fe3–O6	1.979(4)	Fe1···Fe4	3.402(2)
Fe1–O4	1.979(4)	Fe3–O9	2.025(4)	Fe2···Fe3	3.311(1)
Fe1–O7	2.018(5)	Fe3–O11	2.050(5)	Fe3···Fe4	3.440(1)
Fe1–O15	2.022(5)	Fe3–O16	2.053(5)	Fe2···Fe4	6.015(2)
Fe1–O13	2.025(4)	Fe4–O2	1.821(4)	O2–Fe1–O1	83.3(2)
Fe2–O1	1.803(4)	Fe4–O3	2.040(5)	O2–Fe3–O1	83.6(2)
Fe2–O12	2.028(4)	Fe4–O5	2.044(5)	Fe2–O1–Fe1	127.2(2)
Fe2–O14	2.038(4)	Fe4–O18	2.047(5)	Fe2–O1–Fe3	127.0(2)
Fe2–O8	2.047(5)	Fe4–O17	2.162(4)	Fe1–O1–Fe3	97.3(2)
Fe2–O10	2.058(4)	Fe4–N1	2.204(6)	Fe4–O2–Fe3	130.4(2)
Fe2–N4[a]	2.350(5)			Fe4–O2–Fe1	127.6(2)
Fe3–O1	1.897(4)	Fe1···Fe2	3.323(1)	Fe3–O2–Fe1	92.9(2)

[a] $x + ½, -y + {}^3/_2, z + ½$.

Magnetic Studies

Compound **1b** shows a decreasing magnetic susceptibility on cooling from 300 K (Figure 4, a), reaching a minimum of 0.64×10^{-3} cm^3 mol^{-1} at 16 K before increasing on further cooling, and reaching a value of 6.087×10^{-3} cm^{-3} mol^{-1} at 1.9 K. The $\chi T(T)$ plot shows a decreasing value on cooling, reaching a constant value of 0 cm^3 K mol^{-1} at 9 K, thereby indicating a diamagnetic ground state. Given that the $\chi T(T)$ plot is still increasing rapidly around 300 K, the implied size of the magnetic interaction renders a Curie–Weiss fit unworkable, as this equation should be used in temperature ranges approximately ten times the value of the coupling to give a reliable result.

Given the butterfly-type arrangement of this cluster, we can use the following Hamiltonian to describe the system [Equation (1)].

$$H = -J_{bb}(S_A \cdot S_B) - J_{wb}(S_A \cdot S_C + S_A \cdot S_D + S_B \cdot S_C + S_B \cdot S_D) \quad (1)$$

Inspection of the coupling values of similar materials[37] gives a useful starting point for modeling the magnetic susceptibility of **1b**. Using the Magprop program in DAVE CVS,[38] we can use full-matrix diagonalization techniques with a least-squares fitting routine. Fitting a van Vleck equation for a $4 \times S = {}^5/_2$ cluster can be problematical for many commercially available least-squares fitting programs, so matrix techniques can be valuable in this respect.

The results of the fitting procedure show that J_{bb} rapidly increases to $>10^5$ cm^{-1}, whereas J_{wb} remains constant at –88.7 cm^{-1}. The g value in this case was fixed to 2.00, which is reasonable in S = 5/2 ions due to the lack of appreciable spin–orbit coupling or zero-field splitting from the $^6A_1$ ground state of the ion.

An explanation of the value of J_{bb} can be found in fitting the Hamiltonian for this cluster to calculated data. Starting with J_{bb} = 0 cm^{-1} and J_{wb} = –88.7 cm^{-1}, we find that the least-squares fitting procedure has trouble modeling the data. Inspection of the calculated data with increasing values of J_{bb} shows that there is very little difference in the $\chi(T)$ and $\chi T(T)$ plots as a function of J_{bb}, whereby $J_{bb} >$ –10 cm^{-1}. This implies that J_{wb} is the determining factor in the shape of the curve in $\chi(T)$ when J_{bb} is either ferromagnetic or close to zero. This is consistent with other compounds that bear the same $Fe^{III}_4O_2$ center,[37] and we can also see similar behavior in $Cu^{II}_4O_2$ clusters.[39] An estimate for J_{bb} may be made using the formula of Werner et al. [Equation (2)][40] in which d is the average Fe–O distance in the Fe–$(O)_2$–Fe bridge.

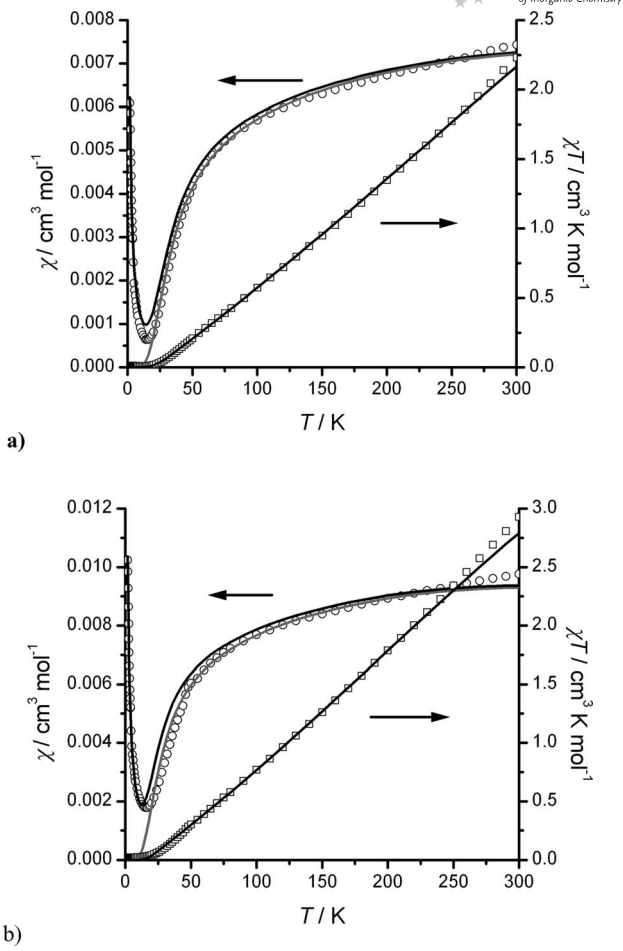

Figure 4. (a) Plot of $\chi(T)$ (black includes a paramagnetic impurity, gray does not) and $\chi T(T)$ for **1b**, with a fit from the matrix diagonalization routine with g = 2.00 (fixed), J_{bb} = 0 cm^{-1} (fixed), and J_{wb} = –88.7 cm^{-1}. (b) The same treatment for **1a**, with g = 2.00 (fixed), J_{bb} = 0 cm^{-1} (fixed), and J_{wb} = –72.2 cm^{-1}.

$$J = -10^7 \times \exp(-6.8d) \text{ cm}^{-1} \quad (2)$$

In **1b**, this would give a coupling of –18.7 cm^{-1}, which would be within the range at which it is not possible to determine the coupling constant through least-squares fitting of the susceptibility data. However, it is possible that this value is only rough given the wide distribution of couplings shown in the study by Werner and co-workers. Additionally, there are also crystallographically distinct clusters present, and as such, the models used above can only be approximations. Compound **1a** (Figure 4, b) presents a similar case with J_{bb} again likely to be near zero and J_{wb} = –72.2 cm^{-1}, respectively.

The susceptibility of compound **2** could not be easily resolved using the above methods, which is surprising, as the Fe–O–Fe angles between wing and body are almost in agreement with the ideal case as described in the Hamiltonian in Equation (1), thus it would be expected that this would be the easiest to fit. However, using the equation of Weihe and Güdel et al.,[41] we are able to make a prediction for the Fe–O–Fe couplings [Equation (3)] in which ϕ is the Fe–O–Fe angle in degrees and r is the average Fe–O bond length in Å.

$$J = -1.337 \times 10^8 \times (3.536 + 2.488\cos\phi + \cos^2\phi) \times \exp(-7.909r) \quad (3)$$

The resulting values (Table 5) from the equation do not give a good fit to the data, but closer inspection of the variation of coupling with distance and angle indicates that the coupling interaction does not scale linearly with r, so that the use of the average Fe–O distance may not give an optimal solution. Instead, we propose that it makes a good upper bound, whereas computing the coupling values for that of the longest Fe–O bond give a lower bound, which in this case models the actual susceptibility well (Figure 5). As the superexchange mechanism does not scale linearly with distance, it is likely that the longest Fe–O distance is the most important one in determining the coupling. As stated in ref.[40–42] the Fe–O–Fe angle is only of second-order importance to the coupling value.

Table 5. Structural parameters and calculated magnetic couplings in **2**, using Equation (3).[41]

	Fe–O1	Fe–O2	Fe–O_{av}	Fe–O–Fe	J_{av}	J_2
Fe4–O1–Fe3	1.821	1.969	1.895	130.4	–97.1	–54.1
Fe4–O1–Fe1	1.821	1.970	1.896	127.6	–98.6	–55.1
Fe2–O2–Fe3	1.802	1.897	1.850	127.0	–142.5	–97.9
Fe2–O2–Fe1	1.802	1.907	1.855	127.2	–136.8	–90.3

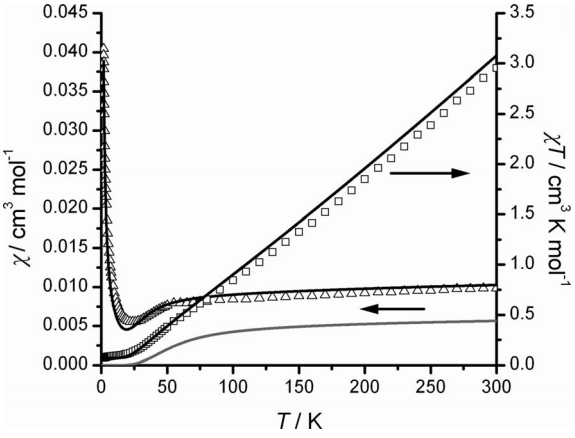

Figure 5. Plot of $\chi(T)$ (black includes a paramagnetic impurity, gray does not) and $\chi T(T)$ for **2**, with models calculated from values obtained from Equation (3). The lower value $\chi(T)$ model uses the average Fe–O bond lengths, whereas the closer-fitting model uses only the longest Fe–O lengths. The $\chi T(T)$ model is from the best J values (see text and Table 5 for details).

The curve obtained with the J_2 values from the lower-bound model produces a good fit when an $S = 5/2$ impurity of 1.6% is added (Figure 5). The best fit is obtained by setting J_{bb} to –22 cm^{-1}, obtained from the model of Werner et al.[40]

In ref.[41] the Fe–O distances are usually shorter than in **1**–**2** and range from 1.747 to 1.839 Å, and the couplings are correspondingly higher (in the range –160 to –265 cm^{-1}). In the study of Werner et al. on di-μ_2-oxo bridges, the distances range from 1.955–2.044 Å with couplings of +1.2 to –28.6 cm^{-1}. The overall trend is that as the bond length increases, the coupling decreases. In the wing–body interactions, we have a combination of the two Fe–O bond types, so it is to be expected that the values obtained from the fits to the data should be in between the two groups. In each case, the ground state of the cluster is $S = 0$, which is common in this type of cluster.[37b] The small tail at low temperature is either a paramagnetic impurity, or in addition, the effect of a small difference in g value between nonequivalent Fe^{III} ions. It is worth mentioning here that the values for J_{wb} in **1a** and **1b** lack error values; modeling these parameters with Magprop gave errors several orders of magnitude larger than the values obtained, although small changes in the coupling values can induce large changes in the model. As such, it is likely that the values are correct to ± 1 cm^{-1}. For compound **2**, we used only the values obtained from Equation (3) and refinement of those values resulted in unstable refinements.

Conclusion

We have described the synthesis, structure, and magnetic properties of three new tetranuclear Fe_4 complexes, all of which have an $\{Fe_4(\mu_3\text{-}O)_2\}^{8+}$ core. Treatment of the trinuclear μ_3-oxo-bridged pivalate complex $[Fe_3O(O_2CCMe_3)_6(H_2O)_3]Me_3CCO_2$ with 2,2′-bipyrimidine results in cluster **1a** $[Fe_4O_2(O_2CCMe_3)_8(bpm)]$. By changing the μ_3-oxo trinuclear precursor to a hexanuclear pivalate complex, using $[Fe_6O_2(OH)_2(O_2CCMe_3)_{12}]$ with 2,2′-bipyrimidine under similar synthetic conditions, we obtained another tetranuclear cluster **1b** with the same composition, but with a different connectivity of metal ions and included solvent molecules. Clusters **1a** and **1b** can also be prepared by microwave heating, thereby resulting in higher yields. Unfortunately, the attempts to prepare Fe_4 cluster-based coordination polymers in which bpm molecules act as bridges were unsuccessful. However, by using hmta as a bridging ligand, a zigzag coordination polymer, $[Fe_4O_2(O_2CCMe_3)_8(hmta)]_n$ (**2**), in which tetranuclear clusters $[Fe_4O_2(O_2CCMe_3)_8]$ are connected by hmta, has been synthesized from a μ_3-oxo trinuclear precursor. The X-ray analysis of the structures of these complexes revealed the differences in the $\{Fe_4(\mu_3\text{-}O)_2\}^{8+}$ core: four Fe atoms in the metal core display a chair conformation in **1a** and **2**, whereas in **1b**, Fe atoms are disposed in a bent butterfly arrangement. The different synthetic routes affect the connectivity of iron atoms in the $Fe_4(\mu_3\text{-}O)_2\}^{8+}$ core, thus allowing us to fine-tune the confor-

mation of this core and the iron–iron distances in it. Magnetochemical analysis of the reported Fe_4 butterfly clusters shows that the antiferromagnetic interactions between wing–body Fe^{III} ions are slightly stronger in **1b** (J_{wb} = –88.7 cm^{-1}) in comparison with wing–body interactions in **1a** (J_{wb} = –72.2 cm^{-1}).

Experimental Section

Materials and Physical Measurements: All reactions were carried out under aerobic conditions using commercial-grade solvents. $[Fe_3O_2(O_2CCMe_3)_6(H_2O)_3]Me_3CCO_2{\cdot}2Me_3CCO_2H$[43] and $[Fe_6O_2(OH)_2(O_2CCMe_3)_{12}]$[44] were synthesized as described elsewhere. The infrared spectra were recorded with a Perkin–Elmer Spectrum One spectrometer using KBr pellets in the region 4000–400 cm^{-1}. Magnetic susceptibility measurements were performed with a Quantum Designs MPMS SQUID-*XL5* magnetometer with an applied field of 1000 G between 300 and 1.9 K. Samples were prepared in Saran film bags. Diamagnetic corrections were applied using the formula 0.45×10^{-6} $cm^3\,mol^{-1}$.[45]

X-ray Crystallography: Single-crystal X-ray studies were carried out with a Nonius KappaCCD and the related analysis software[46] for **1a** at 150 K and with a Stoe Image Plate Diffraction System[47] for **1b**·3MeCN and **2** at 170 K. Details of the crystal, data collection, and refinement parameters are in Table 6. The structures were solved by direct methods and refined by using full-matrix least-squares methods on weighted F^2 values for all reflections using the SHELX suite of programs.[48] The non-hydrogen atoms were refined with anisotropic displacement parameters. Hydrogen atoms except for one of the pivalate ligands in **1b** were placed in fixed, idealized positions and refined as rigidly bonded to the corresponding atom. In compound **1b** two positions have been specified for carbon atoms (C12A, C13A, C14A, and C15A). In this case, the hydrogen atoms of corresponding methyl groups were not localized.

Table 6. Crystal data and details of structural determinations for **1**–**2**.

	1a	**1b**·3MeCN	**2**
Chemical formula	$C_{48}H_{78}Fe_4N_4O_{18}$	$C_{54}H_{87}Fe_4N_7O_{18}$	$C_{46}H_{84}Fe_4N_4O_{18}$
Formula weight	1222.54	1345.71	1204.57
T [K]	150(2)	170(2)	170(2)
λ [Å]	0.71073	0.71073	0.71073
Crystal system	monoclinic	triclinic	monoclinic
Space group	$P2_1/n$	$P\bar{1}$	$P2_1/n$
a [Å]	11.3471(2)	13.8170(15)	14.939(3)
b [Å]	23.9570(3)	22.544(2)	26.386(5)
c [Å]	22.5758(3)	25.581(2)	15.755(3)
α	90	65.674(11)	90
β	96.641(1)	83.638(12)	95.29(3)
γ [°]	90	74.618(12)	90
U [Å^3]	6095.88(15)	7000.7(11)	6184(2)
Z	4	4	4
$D_{calcd.}$ [g cm^{-3}]	1.332	1.277	1.294
μ [mm^{-1}]	0.999	0.877	0.984
R indices [$I>2\sigma(I)$]	R_1 = 0.0444, wR_2 = 0.1044	R_1 = 0.0695, wR_2 = 0.1547	R_1 = 0.0648, wR_2 = 0.1299

CCDC-737575 (for **1a**), -737576 (for **1b**), and -737577 (for **2**) contain the supplementary crystallographic data for this paper. These data can be obtained free of charge from The Cambridge Crystallographic Data Centre via www.ccdc.cam.ac.uk/data_request/cif.

$[Fe_4O_2(O_2CCMe_3)_8(bpm)]$ (1a): This compound was synthesized by using two different methods.

Method A: A solution of 2,2′-bipyrimidine (0.032 g, 0.2 mmol) in MeCN (5 mL) was added to a solution of $[Fe_3O(O_2CCMe_3)_6(H_2O)_3]Me_3CCO_2{\cdot}2Me_3CCO_2H$ (0.230 g, 0.2 mmol) in CH_2Cl_2 (10 mL). The resulting dark brown mixture was heated at reflux for 30 min. Black crystals of complex **1** suitable for X-ray analysis were separated by filtration after two weeks, washed with MeCN, and dried in air; yield 0.110 g, 60%. $C_{48}H_{78}Fe_4N_4O_{18}$ (1222.55): calcd. C 47.16, H 6.43, N 4.58; found C 47.10, H 6.68, N 4.57. IR (KBr): $\tilde{\nu}$ = 3435 (br. m), 2962 (vs), 2928 (sh), 2870 (sh), 1706 (sh), 1566 (vs), 1521 (sh), 1484 (vs), 1422 (vs), 1377 (s), 1362 (s), 1227 (s), 1169 (w), 1112 (w), 1098 (w), 1030 (w), 1012 (w), 937 (w), 906 (w), 826 (w), 814 (w), 789 (w), 764 (w), 691 (w), 657 (m), 606 (s), 518 (w), 439 (m) cm^{-1}.

Method B: A solution of $[Fe_3O_2(O_2CCMe_3)_6(H_2O)_3]Me_3CCO_2{\cdot}2Me_3CCO_2H$ (0.230 g, 0.2 mmol) and 2,2′-bipyrimidine (0.032 g, 0.2 mmol) in MeCN (4 mL) was heated at 160 °C for 20 min in a microwave reactor. Black crystals of **1a** suitable for X-ray analysis were separated by filtration after 5 d, washed with MeCN, and dried in air; yield 0.142 g, 78%. $C_{48}H_{78}Fe_4N_4O_{18}$ (1222.55): calcd. C 47.16, H 6.43, N 4.58; found C 47.13, H 6.46, N 4.55. The identity of **1a** was established by comparison of IR data as well as elemental and TG analysis.

$[Fe_4O_2(O_2CCMe_3)_8(bpm)]$ (1b·3MeCN): This compound was synthesized by using two different methods.

Method A: A solution of 2,2′-bipyrimidine (0.032 g, 0.2 mmol) in 5 mL MeCN was added to a solution of $[Fe_6O_2(OH)_2(O_2CCMe_3)_{12}]$ (0.08 g, 0.05 mmol) in CH_2Cl_2 (5 mL). The resulting dark brown solution was allowed to stand at room temperature. Black crystals of complex **1b** suitable for X-ray analysis were separated by filtration after one week, washed with MeCN, and dried in air; yield 0.02 g, 22%. Complex **1b** ($C_{48}H_{78}Fe_4N_4O_{18}$) solvent free: calcd. C 47.16, H 6.43, N 4.58; found C 47.51, H 6.59, N 4.40. IR (KBr): $\tilde{\nu}$ = 3435 (br. m), 2962 (vs), 2928 (sh), 2870 (sh), 1706 (sh), 1566 (vs), 1521 (sh), 1484 (vs), 1422 (vs), 1377 (s), 1362 (s), 1227 (s), 1169 (w), 1112 (w), 1098 (w), 1030 (w), 1012 (w), 937 (w), 906 (w), 826 (w), 814 (w), 789 (w), 764 (w), 691 (w), 657 (m), 606 (s), 518 (w), 439 (m) cm^{-1}.

Method B: A solution of $[Fe_6O_2(OH)_2(O_2CCMe_3)_{12}]$ (0.161 g, 0.1 mmol) and 2,2′-bipyrimidine (0.023 g, 0.15 mmol) in MeCN (4 mL) was heated at 160 °C for 20 min in a microwave synthesizer. Black crystals of **1b** were separated by filtration after 3 d, washed with MeCN, and dried in air; yield 0.102 g, 56%. Complex **1b** ($C_{48}H_{78}Fe_4N_4O_{18}$) solvent free: calcd. C 47.16, H 6.43, N 4.58; found C 47.00, H 6.59, N 4.59. The identity of **1b** was established by comparison of IR data as well as elemental and TG analysis.

$[Fe_4O_2(O_2CCMe_3)_8(hmta)]_n$ (2): A solution of hexamethylenetetramine (0.042 g, 0.3 mmol) in MeCN (5 mL) was added to a solution of $[Fe_3O(O_2CCMe_3)_6(H_2O)_3]Me_3CCO_2{\cdot}2Me_3CCO_2H$ (0.230 g, 0.2 mmol) in MeCN (10 mL). The resulting dark brown mixture was stirred for 2 h. Black crystals of complex **2** suitable for X-ray analysis were separated by filtration after three weeks, washed with hexane, and dried in air; yield 0.08 g, 35%. $C_{46}H_{84}Fe_4N_4O_{18}$ (1204.57): calcd. C 45.87, H 7.02, N 4.65; found C 46.05, H 6.54, N 4.54. IR (KBr): $\tilde{\nu}$ = 2962 (vs), 2930 (sh), 2873 (sh), 1574 (sh), 1547 (vs), 1512 (m), 1485 (vs), 1459 (m), 1419 (vs), 1375 (m), 1362 (m), 1250 (m), 1228 (s), 1056 (w), 1024 (m), 988 (m), 905 (w), 788 (w), 768 (w), 686 (m), 603 (m), 536 (w), 435 (m) cm^{-1}.

Supporting Information (see also the footnote on the first page of this article): Packing diagram for **1a** (Figure S1), **1b** (Figure S2), and **2** (Figure S3).

Acknowledgments

This work was supported by the Swiss National Science Foundation (SCOPES IB7320-110976/1 and IZ73Z0_127925).

[1] a) S. R. Batten, R. Robson, *Angew. Chem. Int. Ed.* **1998**, *37*, 1460–1494; b) P. J. Hagrman, D. Hargman, J. Zubieta, *Angew. Chem. Int. Ed.* **1999**, *38*, 2638–2684; c) A. J. Blake, N. R. Champness, P. Hubberstey, W.-S. Li, M. A. Withersby, M. Schroder, *Coord. Chem. Rev.* **1999**, *183*, 117–138; d) R. Robson, *J. Chem. Soc., Dalton Trans.* **2000**, 3735–3744; e) M. Eddaoudi, D. B. Moler, H. Li, B. Chen, T. M. Reineke, M. O'Keeffe, O. M. Yaghi, *Acc. Chem. Res.* **2001**, *34*, 319–330; f) B. Moulton, M. J. Zaworotko, *Chem. Rev.* **2001**, *101*, 1629–1658; g) B. Moulton, M. J. Zaworotko, *Curr. Opin. Solid State Mater. Sci.* **2002**, *6*, 117–123; h) Ch. Janiak, *Dalton Trans.* **2003**, 2781–2804; i) O. M. Yaghi, M. O'Keeffe, N. W. Ockwig, H. K. Chae, M. Eddaoudi, J. Kim, *Nature* **2003**, *423*, 705–714; j) A. K. Cheetham, C. N. R. Rao, R. K. Feller, *Chem. Commun.* **2006**, 4780–4795; k) U. Mueller, M. Schubert, F. Teich, H. Puetter, K. Schierle-Arndt, J. Pastre, *J. Mater. Chem.* **2006**, *16*, 626–636; l) M. Andruh, *Chem. Commun.* **2007**, 2565–2577; m) B. Wang, A. P. Cote, H. Furukawa, M. O'Keeffe, O. M. Yaghi, *Nature* **2008**, *453*, 207–211.

[2] a) A. W. C. Berg, C. O. Area, *Chem. Commun.* **2008**, 668–681; b) M. Dinca, J. R. Long, *Angew. Chem. Int. Ed.* **2008**, *47*, 6766–6779; c) Y. Kubota, M. Takata, T. C. Kobayashi, S. Kitagawa, *Coord. Chem. Rev.* **2007**, *251*, 2510–2521; d) H. Furukawa, M. A. Miller, O. M. Yaghi, *J. Mater. Chem.* **2007**, *17*, 3197–3204; e) N. L. Rosi, J. Eckert, M. Eddaoudi, D. T. Vodak, J. Kim, M. O'Keeffe, O. M. Yaghi, *Science* **2003**, *300*, 1127–1129; f) L. J. Murray, M. Dinca, J. R. Long, *Chem. Soc. Rev.* **2009**, *38*, 1294–1314.

[3] a) D. Maspoch, D. Ruiz-Molina, J. Veciana, *J. Mater. Chem.* **2004**, *14*, 2713–2723; b) M. Kurmoo, *Chem. Soc. Rev.* **2009**, *38*, 1353–1379.

[4] a) N. L. Rosi, M. Eddaoudi, J. Kim, M. O'Keefee, O. M. Yaghi, *CrystEngComm* **2002**, *4*, 401–404; b) D. J. Tranchemontagne, J. L. Mendoza-Cortes, M. O'Keefee, O. M. Yaghi, *Chem. Soc. Rev.* **2009**, *38*, 1257–1283; c) J. J. Perry IV, J. A. Perman, M. J. Zaworotko, *Chem. Soc. Rev.* **2009**, *38*, 1400–1417.

[5] a) M. Soler, E. Rumberger, K. Folting, D. N. Hendrickson, G. Christou, *Polyhedron* **2001**, *20*, 1365–1369; b) D. J. Price, S. R. Batten, B. Moubaraki, K. S. Murray, *Chem. Commun.* **2002**, 762–763; c) E. K. Brechin, C. Boskovic, W. Wernsdorfer, J. Yoo, A. Yamaguchi, E. C. Sanado, T. R. Concolino, A. L. Rheingold, H. Ishimoto, D. N. Hendrickson, G. Christou, *J. Am. Chem. Soc.* **2002**, *124*, 9710–9711; d) M. Soler, W. Wernsdorfer, K. Folting, M. Pink, G. Christou, *J. Am. Chem. Soc.* **2004**, *126*, 2156–2165; e) M. Murugesu, M. Habrych, W. Wernsdorfer, K. A. Abboud, G. Christou, *J. Am. Chem. Soc.* **2004**, *126*, 4766–4767; f) A. J. Tasiopoulos, A. Vinslave, W. Wernsdorfer, K. A. Abboud, G. Christou, *Angew. Chem. Int. Ed.* **2004**, *43*, 2117–2121; g) E. C. Sanudo, W. Wernsdorfer, K. A. Abboud, G. Christou, *Inorg. Chem.* **2004**, *43*, 4137–4144; h) M. Murugesu, J. Raftery, W. Wernsdorfer, G. Christou, E. K. Brechin, *Inorg. Chem.* **2004**, *43*, 4203–4209; i) P. King, W. Wernsdorfer, K. A. Abboud, G. Christou, *Inorg. Chem.* **2004**, *43*, 7315–7323; j) A. J. Tasiopoulos, W. Wernsdorfer, K. A. Abboud, G. Christou, *Inorg. Chem.* **2005**, *44*, 6324–6338; k) P. King, W. Wernsdorfer, K. A. Abboud, G. Christou, *Inorg. Chem.* **2005**, *44*, 8659–8669; l) G. Christou, *Polyhedron* **2005**, *24*, 2065–2075; m) Y. Li, W. Wernsdorfer, R. Clerac, I. J. Hewitt, C. E. Anson, A. K. Powell, *Inorg. Chem.* **2006**, *45*, 2376–2378; n) T. C. Stamatatos, K. A. Abboud, W. Wernsdorfer, G. Christou, *Angew. Chem. Int. Ed.* **2007**, *46*, 884–888; o) C.-I. Yang, W. Wernsdorfer, G.-H. Lee, H.-L. Tsai, *J. Am. Chem. Soc.* **2007**, *129*, 456–457; p) C. J. Milios, R. Inglis, R. Bagai, W. Wernsdorfer, A. Collins, S. Moggach, S. Parsons, S. P. Perlepes, G. Christou, E. K. Brechin, *Chem. Commun.* **2007**, 3476–3478; q) L. Bogani, W. Wernsdorfer, *Nat. Mater.* **2008**, *7*, 179–186.

[6] S. G. Baca, I. L. Malaestean, T. D. Keene, H. Adams, M. D. Ward, J. Hauser, A. Neels, S. Decurtins, *Inorg. Chem.* **2008**, *47*, 11108–11119.

[7] P. Albores, E. Rentschler, *Inorg. Chem.* **2008**, *47*, 7960–7962.

[8] S. W. Przybylak, F. Tuna, S. J. Teat, R. E. P. Winpenny, *Chem. Commun.* **2008**, 1983–1985.

[9] D. R. Turner, S. N. Pek, J. D. Cashion, B. Moubaraki, K. S. Murray, S. R. Batten, *Dalton Trans.* **2008**, 6877–6879.

[10] a) G. B. Deacon, R. J. Philips, *Coord. Chem. Rev.* **1980**, *33*, 227–250; b) R. C. Mehrotra, R. Bohra, *Metal Carboxylates*, Academic Press, New York, **1983**; c) K. Nakamoto, *Infrared and Raman Spectra of Inorganic and Coordination Compounds*, Wiley, New York, **1986**, p. 236.

[11] a) M. Julve, M. Verdaguer, G. De Munno, J. A. Real, G. Bruno, *Inorg. Chem.* **1993**, *32*, 795–802; b) E. Andres, G. De Munno, M. Julve, J. A. Real, F. Lloret, *J. Chem. Soc., Dalton Trans.* **1993**, 2169–2174; c) D. Armentano, G. De Munno, F. Lloret, M. Julve, J. Curely, A. M. Babb, J. Y. Lu, *New J. Chem.* **2003**, *27*, 161–165; d) D. Armentano, G. De Munno, F. Guerra, J. Faus, F. Lloret, M. Julve, *Dalton Trans.* **2003**, 4626–4634; e) A. K. Boudalis, C. P. Raptopoulou, A. Terzis, S. P. Perlepes, *Polyhedron* **2004**, *23*, 1271–1277.

[12] I. S. Ahuja, R. Singh, C. L. Yadava, *Proc. Indian Acad. Sci. (Chem. Sci.)* **1983**, *92*, 59–64.

[13] F. H. Allen, *Acta Crystallogr., Sect. B* **2002**, *58*, 380–388.

[14] M. W. Wemple, D. K. Coggin, J. B. Vincent, J. K. McCusker, W. E. Streib, J. C. Huffman, D. N. Hendrickson, G. Christou, *J. Chem. Soc., Dalton Trans.* **1998**, 719–726.

[15] A. K. Boudalis, V. Tangoulis, C. P. Raptopoulou, A. Terzis, J.-P. Tuchagues, S. P. Perlepes, *Inorg. Chim. Acta* **2004**, *357*, 1345–1354.

[16] T. C. Stamatatos, A. K. Boudalis, Y. Sanakis, C. P. Raptopoulou, *Inorg. Chem.* **2006**, *45*, 7372–7381.

[17] J. Overgaard, D. E. Hibbs, E. Rentschler, G. A. Timco, F. K. Larsen, *Inorg. Chem.* **2003**, *42*, 7593–7601.

[18] S. M. Gorun, S. J. Lippard, *Inorg. Chem.* **1988**, *27*, 149–156.

[19] W. H. Armstrong, M. E. Roth, S. J. Lippard, *J. Am. Chem. Soc.* **1987**, *109*, 6318–6326.

[20] J. K. McCusker, J. B. Vincent, E. A. Schmitt, M. L. Mino, K. Shin, D. K. Coggin, P. M. Hagen, J. C. Huffman, G. Christou, D. N. Hendrickson, *J. Am. Chem. Soc.* **1991**, *113*, 3012–3021.

[21] B. Yan, Z.-D. Chen, *Inorg. Chem. Commun.* **2001**, *4*, 138–141.

[22] P. Chaudhuri, M. Winter, P. Fleischhauer, W. Haase, U. Florke, H.-J. Haupt, *Inorg. Chim. Acta* **1993**, *212*, 241–249.

[23] R. A. Reynolds, W. R. Dunham, D. C. Coucouvanis, *Inorg. Chem.* **1998**, *37*, 1232–1241.

[24] C. Dendrinou-Samara, S. Katsamakas, C. Raptopoulou, A. Terzis, V. Tangoulis, D. P. Kessissoglou, *Polyhedron* **2007**, *26*, 763–772.

[25] P. Chaudhuri, E. Rentschler, F. Birkelbach, C. Krebs, E. Bill, T. Weyhermuller, U. Florke, *Eur. J. Inorg. Chem.* **2003**, 541–555.

[26] A. K. Boudalis, N. Lalioti, G. A. Spyroulias, C. P. Raptopoulou, A. Terzis, A. Bousseksou, V. Tangoulis, J.-P. Tuchagues, S. P. Perlepes, *Inorg. Chem.* **2002**, *41*, 6474–6487.

[27] R. Celenligil-Cetin, R. J. Staples, P. Stavropoulos, *Inorg. Chem.* **2000**, *39*, 5838–5846.

[28] V. I. Ponomarev, L. O. Atovmyan, S. A. Bobkova, K. I. Turte, *Dokl. Akad. Nauk SSSR (Russ.)* **1984**, *274*, 368–372.

[29] J. Bacsa, H. Zhao, K. R. Dunbar, *Acta Crystallogr., Sect. C: Cryst. Struct. Commun.* **2003**, *59*, m561–m564.

[30] F. Marchetti, F. Marchetti, B. Melai, G. Pampaloni, S. Zacchini, *Inorg. Chem.* **2007**, *46*, 3378–3384.

[31] X.-F. Yu, W.-Y. Pan, *Jiegou Huaxue* **1993**, *12*, 271–276.

[32] L. Wu, M. Pressprich, P. Coppens, M. J. DeMarco, *Acta Crystallogr., Sect. C: Cryst. Struct. Commun.* **1993**, *49*, 1255–1258.

[33] P. Cortes, A. M. Atria, M. T. Garland, R. Baggio, *Acta Crystallogr., Sect. C: Cryst. Struct. Commun.* **2006**, *62*, m297–m302.

[34] A. Dimitrakopoulou, C. Dendrinou-Samara, A. A. Pantazaki, C. Raptopoulou, A. Terzis, E. Samaras, D. P. Kessissoglou, *Inorg. Chim. Acta* **2007**, *360*, 546–556.
[35] X.-F. Yu, Y.-Q. Jiang, *Huahue Xuebao* **1993**, *51*, 579–585.
[36] S.-Z. Hu, *Jiegou Huaxue* **1999**, *18*, 476–482.
[37] See, for example (and the references therein): a) A. K. Boudalis, N. Lalioti, G. A. Spyroulias, C. Raptopoulou, A. Terzis, A. Bousseksou, V. Tangoulis, J.-P. Tuchagues, S. P. Perlepes, *Inorg. Chem.* **2002**, *41*, 6474–6487; b) T. C. Stamatatos, A. K. Boudalis, Y. Sanakis, C. P. Raptopoulou, *Inorg. Chem.* **2006**, *45*, 7372–7381; c) S. Gomez-Coca, T. Cauchy, E. Ruiz, *Dalton Trans.* **2010**, *39*, 4832–4837.
[38] DAVE: A comprehensive software suite for the reduction, visualization, and analysis of low-energy neutron spectroscopic data: R. T. Azuah, L. R. Kneller, Y. Qiu, P. L. W. Tregenna-Piggott, C. M. Brown, J. R. D. Copley, R. M. Dimeo, *J. Res. Natl. Inst. Stan. Technol.* **2009**, *114*, 341–358.
[39] Y.-H. Deng, J. Liu, B. Wu, C. Ambrus, T. D. Keene, O. Waldmann, S.-X. Liu, S. Decurtins, X.-J. Yang, *Eur. J. Inorg. Chem.* **2008**, 1712–1718.
[40] R. Werner, S. Ostrovsky, K. Griesar, W. Haase, *Inorg. Chim. Acta* **2001**, *326*, 78–88.
[41] H. Weihe, H. U. Güdel, *J. Am. Chem. Soc.* **1997**, *119*, 6539–6543.
[42] C. Cañada-Vilata, T. A. O'Brien, E. K. Brechin, M. Pink, E. R. Davidson, G. Christou, *Inorg. Chem.* **2004**, *43*, 5505–5521.
[43] N. V. Gerbeleu, A. S. Batsanov, G. A. Timko, Iu. T. Struchkov, K. M. Indrichan, G. A. Popovich, *Dokl. Akad. Nauk SSSR (Russ.)* **1987**, *293*, 364–367.
[44] A. S. Batsanov, Iu. T. Struchkov, G. A. Timko, *Koord. Khim.* **1988**, *14*, 266–270.
[45] O. Kahn, *Molecular Magnetism*, VCH Publishers, Inc., New York, **1993**.
[46] *NONIUS*, Kappa CCD Program Package: COLLECT, DENZO, SCALEPACK, SORTAV, Nonius BV, Delft, The Netherlands, **1999**.
[47] *Stoe&Cie IPDS Software*, Stoe&Cie GmbH, Darmstadt, Germany, **2000**.
[48] G. M. Sheldrick, *SHELXS-97* and *SHELXL-97*, University of Göttingen, Germany, **2003**.

Received: August 4, 2010
Published Online: December 9, 2010

